

## Distribution characteristics of falling film thickness on horizontal tube evaporators

El-Sayed R. Negeed<sup>a,b,\*</sup>, F. Mansour<sup>b</sup>

<sup>a</sup>Department of Mechanical Engineering, Faculty of Engineering, King Abdulaziz University, P.O. Box: 80204, Jeddah 21589, Saudi Arabia, email: [ernegeed@kau.edu.sa](mailto:ernegeed@kau.edu.sa)/[s.negeed@gmail.com](mailto:s.negeed@gmail.com)

<sup>b</sup>Reactors Department, Nuclear Research Center, Atomic Energy Authority, P.O. Box: 13759 Cairo, Egypt, email: [fouad\\_ali@yahoo.com](mailto:fouad_ali@yahoo.com)

Received 12 May 2020; Accepted 14 December 2020

---

### ABSTRACT

The aim of this study is to examine experimentally the thickness variations of a falling film on plain and hydrophilic horizontal tube evaporator surfaces in order to enhance the performance of the horizontal tube evaporators. The hydrophilic surfaces are acquired by exposing them to plasma irradiation for a 120 s time period. A test loop has been installed, and by using electrical film thickness measuring devices, the distributions of the formed liquid thickness layer around the hot plain and hydrophilic surfaces are determined at different operating conditions. By analyzing the experimental data, the present results show that the film thickness around the hydrophilic tube changes with the same pattern around the plain tube. The film distribution along the peripheral angle is non-symmetrical, minimum film thickness values are more likely to appear at a different angular position of 90°–120° under various conditions. The film thickness is significantly decreased for hydrophilic surfaces. The film thickness mainly increases as the flow rate increases, while it decreases as the tube diameter increases, the evaporation pressure increases, the inlet water sub-cooling increases, and tube surface temperature increases. The feeder height has a minor influence on the film thickness. Comparison between the current results and results acquired by another researcher is in good agreement between 2.0% and 18%.

*Keywords:* Horizontal tube evaporator; Liquid film thickness; Liquid film on hydrophilic surfaces

---

### 1. Introduction

As of late, falling-film horizontal-tube evaporators have become progressively transcendent in thermal water treatment processes, and thermal desalination industries. That is due to their high heat transfer efficiencies, small temperature differences and thin liquid films. In falling film evaporation, the feeding fluid is spread over the top of the evaporator tubes by a distributor hose or spray nozzle, creating thin films of liquid around the tubes. The heat transfer process of the thin film evaporation takes place when the fluid is flowing downwards on the heated tubes.

The heat transfer mechanism of the thin film evaporation is regulated by boiling nucleates when bubbles form on the surface of the heating tube, and convection throughout the film as direct evaporation occurs at the liquid-vapor interface where a phase change occurs at the interface, and whose magnitude is directly related to the liquid film's shape and thickness. It is possible to use the distribution of the falling film around a horizontal tube for predicting the uniformity of the flow and dry out, to prevent the evaporator tubes from drying out; it is important to completely cover the evaporator tube with a liquid film.

---

\* Corresponding author.

The falling film thickness is reversely proportional to the local heat transfer coefficient, therefore it is an important factor for falling film evaporator design, and the research on the falling film thickness distribution is a valuable method to improve the performance of the horizontal tube evaporators. The nozzles type, and how the liquid film falls from one tube to another are valuable parameters for controlling the film shape and its distribution around the evaporator tubes, [1–5].

The liquid film on the evaporator tube surface directly affects the performance of the horizontal tube evaporators. The maximum spread and the evaporation time of a falling film on hot surfaces depend primarily on the hot surface temperature, liquid viscosity, surface tension, impinging velocity, the contact angle between the liquid and surface, and surface wettability, Negeed et al. [6,7]. The interfacial waves presented on the thin liquid film have a strong impact on the evaporation rate because the interfacial area is increased and therefore the convective heat transfer near the interface is improved, Shahzad et al. [8]. The performance of the horizontal-tube evaporator is significantly affected by the falling flow rate. Ribatski and Jacobi [4] observed three specific flow patterns that depend on the flow rate; discrete droplets, jets or continuous sheets. Awad and Negeed [9–11] have studied experimentally and numerically the falling film on the horizontal tube evaporator. Some significant results obtained in these studies are that very thin stable film on the surfaces of heat transfer greatly improves the performance of the falling film evaporator. For the same vertical column, the film thickness of the upper tube is higher than the film thickness of the lower tubes; this is due to the volatilization of the falling rate from the upper tubes. The condensing film thickness on a vertical plate was analytically solved by Nusselt [12] by neglecting surface tension and inertia forces. Chyu and Bergles [13] correlated the film thickness on a horizontal tube on the basis of Nusselt's solution [12] as follows:

$$\delta = \left( \frac{3\mu_l \Gamma}{\rho_l(\rho_l - \rho_v)g(\pi\theta/180)} \right)^{1/3} \quad (1)$$

where  $\Gamma$  is the flow rate on tube one side and the number of Reynolds is defined as:

$$\text{Re} = \frac{4\Gamma}{\mu_l} \quad (2)$$

Based on Nusselt's solution [12], Hou et al. [14] correlated the film thickness on a horizontal tube with considering the effect of tube spacing,  $s$ , as:

$$\delta = C \left( \frac{3\mu_l \Gamma}{\rho_l(\rho_l - \rho_v)g(\pi\theta/180)} \right)^{1/3} \left( \frac{s}{d_{ot}} \right)^n \quad (3)$$

where  $C = 0.9754$ ,  $n = -0.1667$  for  $0^\circ < \theta \leq 90^\circ$ , and  $C = 0.84978$ ,  $n = -0.16479$  for  $90^\circ < \theta \leq 180^\circ$ .

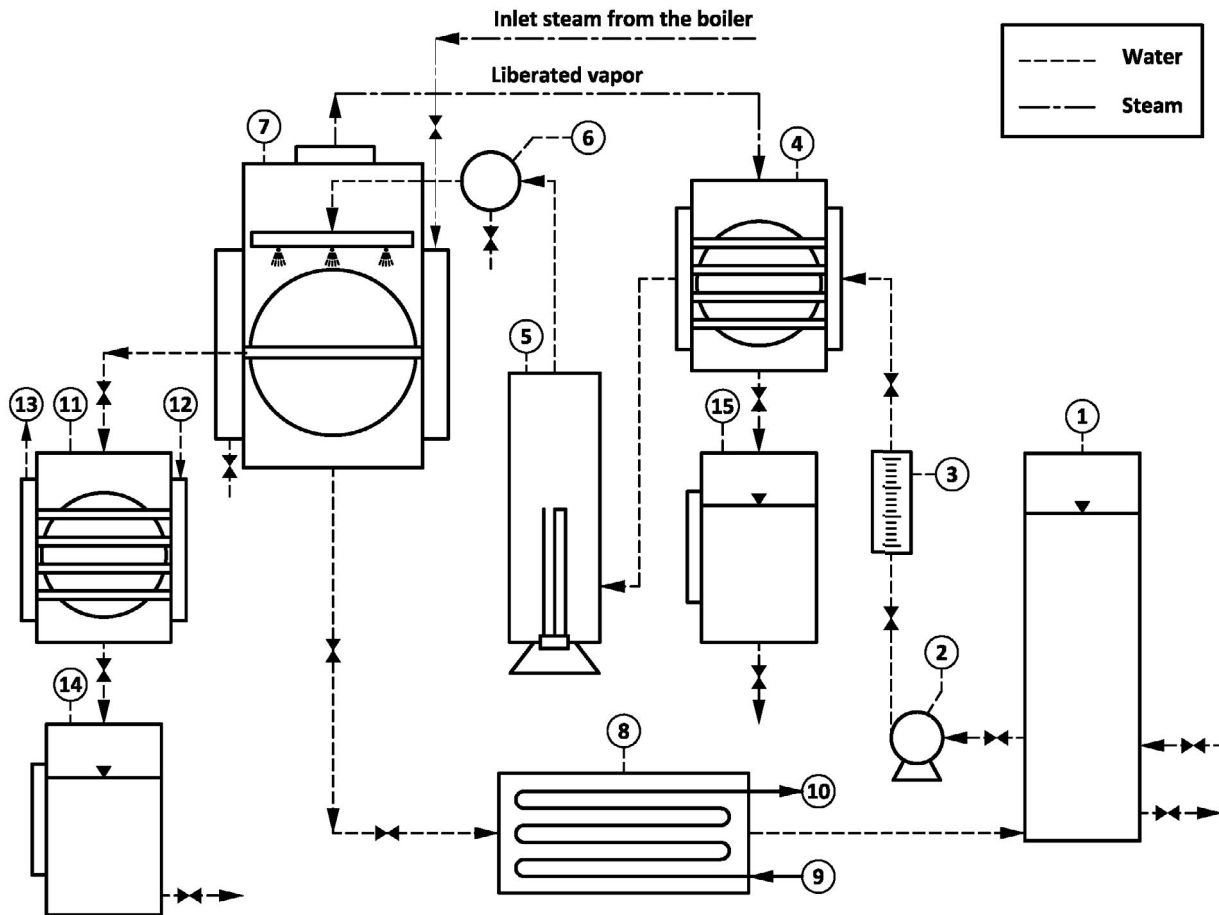
Researchers [15–19] showed that the film distribution at the peripheral angle of the tube surface is non-symmetrical

and under different conditions, the minimum film thickness values appeared to occur at various angular locations from  $110^\circ$  to  $150^\circ$  [15],  $100^\circ$ – $140^\circ$  [16],  $110^\circ$ – $150^\circ$  [17],  $95^\circ$ – $120^\circ$  [18], and  $90^\circ$ – $100^\circ$  [19]. Numerically, Luo et al. [20] showed that, at the angular angle of  $125^\circ$ ,  $160^\circ$  and  $170^\circ$ , the minimum liquid film thickness of the circular tube, the oval-shaped tube and the drop-shaped tube respectively appear.

The distribution characteristics of falling film thickness on horizontal tube evaporators have been intensively studied in recent decades and are still the subject of many ongoing research activities to optimize knowledge of heat transfer processes for boiling/evaporation and to improve the performance of their applications. Despite this effort, many aspects of heat transfer boiling/evaporation are still not fully understood; the difficulty is due mainly to the small time and length scales. To give a superior comprehension of the general execution and increase further understanding of the local heat and mass transfer of the falling film horizontal tube evaporators, the falling film distributions around the horizontal tube evaporators ought to be dependable anticipated. From the above writing survey, the falling film heat transfer of horizontal tube evaporators stays important to researchers because of the multifaceted nature of these phenomena. However, little literature on hydrophilic horizontal tube evaporators focused on the distribution characteristics of falling film thickness. The objective of this research study is to analyze experimentally the thickness variations of a falling film on plain and hydrophilic horizontal tube evaporators to give a superior comprehension of heat and mass exchange processes in horizontal tube evaporators. The impacts of hydrophilic surfaces, operating parameters, and evaporator design on the thickness variations of the falling film formed around the horizontal tube evaporators were researched.

## 2. Experimental work

Fig. 1 displays the experimental setup's schematic diagram. The pump (2) pushes the feed water from the constant water path (1) to the primary heater (4), where heated by the latent heat of the released vapor, then the feed water is heated by an electric heater to different temperatures (5). A thermostat controls the various temperatures. Water enters the test chamber through the nozzles distributor at different temperatures that can be controlled by a thermostat. Through the nozzle distributor (6), the feedwater enters the test chamber (7) and then falls to the test heated tube using the fan-jet flat to achieve uniform distribution. The pressure inside the test chamber is controlled using a vacuum pump. To maintain constant surface temperature during the tests, dry saturated steam from the boiler is used to heat the test tube. For this system, a fire tube boiler with a saturated or superheated steam capacity of 2.0 t/h at a maximum pressure of 10 bar is used. The exiting steam from the tube passes through the condenser (11) where it is condensed and then is measured by the collecting tank (14). Released vapor from the test chamber condenses in the primary heater (4) and then measured by a calibrated tank (15). In the cooler (8), the non-evaporated spray water is cooled and returned to the water bath at constant temperature (1). The feed flow rate is measured by a rotameter (3).



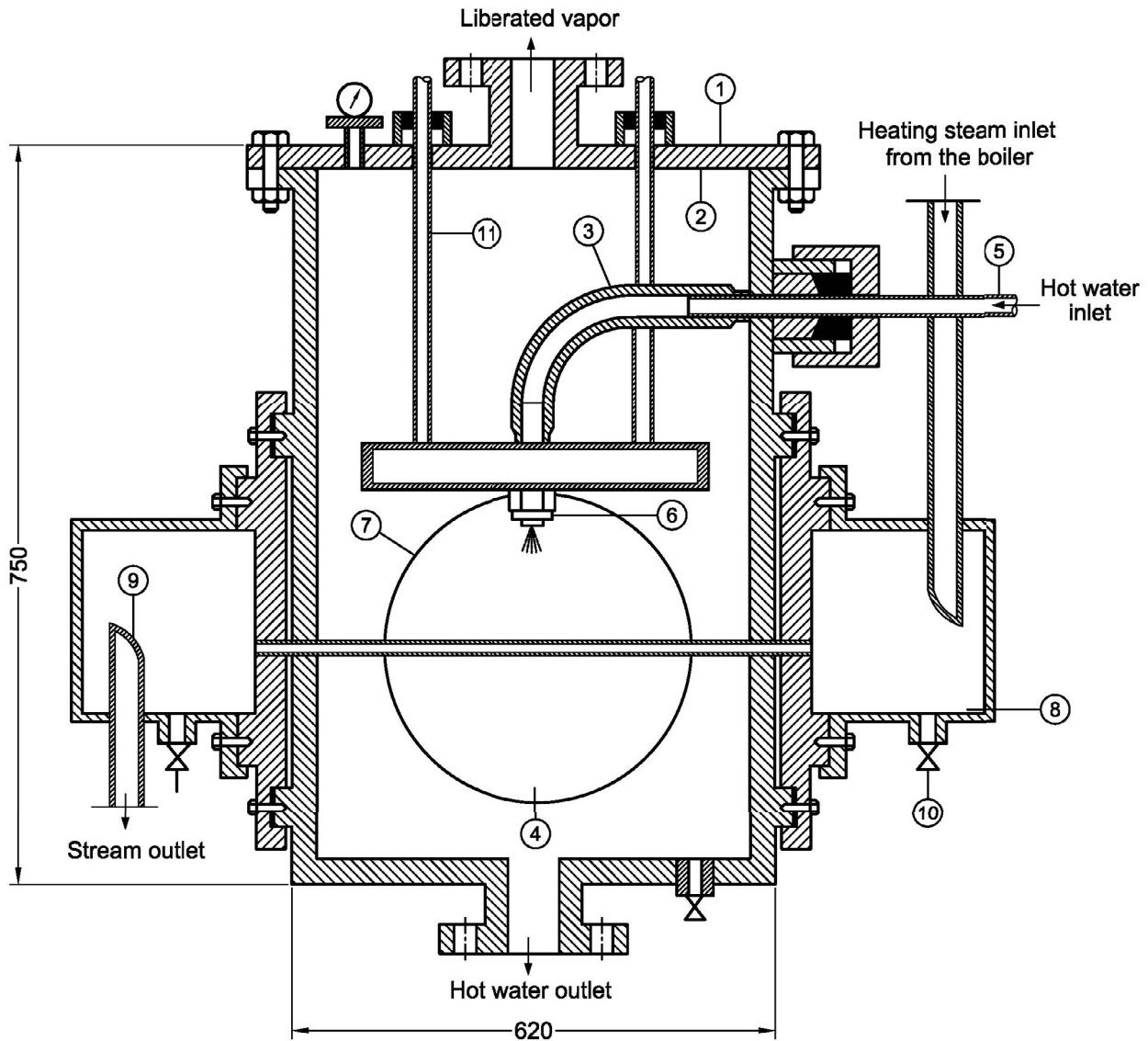
- |                                    |                          |                         |
|------------------------------------|--------------------------|-------------------------|
| 1. Constant temperature water bath | 6. Hot water distributor | 11. Condenser Inlet     |
| 2. Circulating pump                | 7. Test chamber          | 12. Cooled water        |
| 3. Rotameter                       | 8. Cooler                | 13. Outlet cooled water |
| 4. Primary tank                    | 9. Inlet cooled water    | 14. Calibrated tan      |
| 5. Electrical heater               | 10. Outlet cooled water  | 15. Condensate tank     |

Fig. 1. Line diagram of the experimental setup.

Fig. 2 shows the sectional view of the test chamber. The nominal dimensions of the stainless steel test chamber are 50 cm × 62 cm × 75 cm and 5 mm wall thickness. For visual observation of the distribution of the liquid film around the tube surfaces and sprayed liquid characteristics, there are two Pyrex windows of 25 cm diameter. Moving the distributor up and down through two grooves at the top of the test chamber changes the falling distance. Fan-jet flat-spray type nozzles produced by Steinen Co., USA have been used to spray the feed water on the tubes. The nozzle consists of four main components: cap, orifice tip, 100-measure stainless steel screen strainer and adapter. The test tubes are made of copper.

The experimental runs were performed by spraying heated water on plain and hydrophilic tube surfaces, where,

the inlet water temperature, surface temperature and flow rate were independently controlled. The hydrophilic surface treatment will be accomplished by 120 s exposure of the tubes to plasma irradiation. The plasma irradiated solid surfaces become hydrophilic. This is because the particles of plasma remove the layer of gas absorption and the active layer of oxide appears on the surface. These effects of rinsing and activating change the surface and improve its wettability. Wettability Reformer ST-700 produced by Keyence Corp. is the plasma generator used in the current experiments and its generated power is 200 W. More description of the plasma generator is shown in Negeed et al. [6]. Fig. 3 shows the scanning electron microscopy images of the plain and hydrophilic tube surfaces, where Fig. 4 shows the photographs of the copper tube of 1.0-inch diameter



- |                   |                           |                                 |
|-------------------|---------------------------|---------------------------------|
| 1. Demister plate | 5. Three channels         | 9. Outlet steam chamber         |
| 2. Rubber gasket  | 6. Three spraying nozzles | 10. Vent valve                  |
| 3. Rubber tube    | 7. Nine testing tubes     | 11. Nozzles distributor carrier |
| 4. Pyrex windows  | 8. Inlet steam chamber    |                                 |

Fig. 2. A sectional view of the test chamber.

and 0.5 m length of plain surface and surface treated by exposing them to plasma irradiation.

The pressure and temperature of the inlet and outlet are determined for each section. The falling film thicknesses around the surface are measured at different angular positions (30°, 60°, 90°, 120°, 150°) by using electric film thickness-measuring probes. The probe as shown in Fig. 5 consists of a depth micrometer, a spatial mechanism to transfer the rotating movement of the micrometer to axial movement, a stainless steel needle, and an

electrical contact circuit for viewing the film thickness. The needle is adjusted to touch on the outer tube surfaces, and the needle is slowly passed across the water film by the spatial mechanism. Whenever the needle is located through the liquid film, the electrical circuit becomes operational. If the needle comes out of the liquid film, the circuit will be disconnected, then the thickness of the film around the surface is then determined by the micrometer. Copper-constantan sheathed thermocouples; type *T* of 0.5 mm diameter are used for measuring all the temperature.

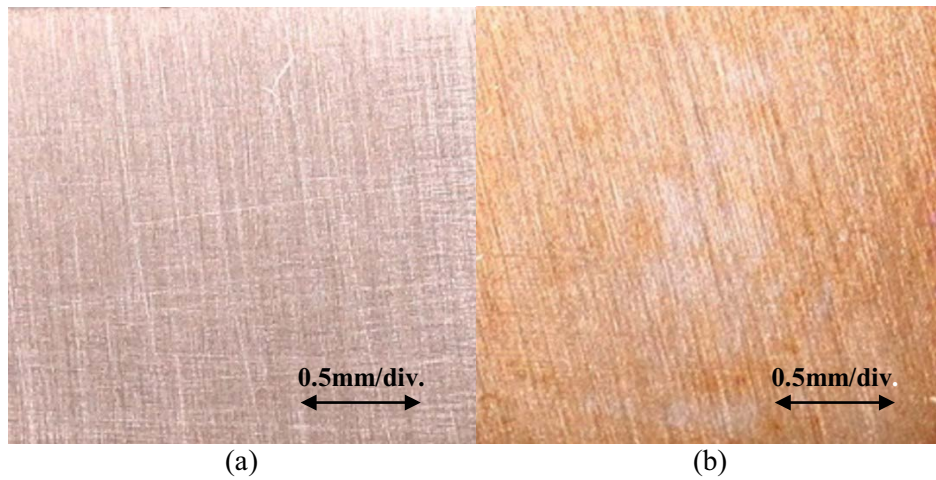


Fig. 3. Scanning electron microscopy photographs of the copper: (a) plain surface and (b) surface treated by exposing them to plasma irradiation for about different exposure durations 120 s.

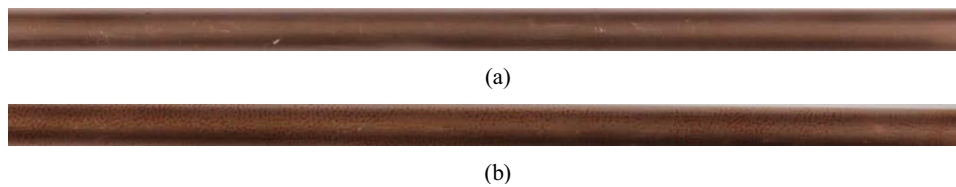


Fig. 4. Photographs of the copper tube: (a) plain surface and (b) surface treated by exposing them to plasma irradiation for 120 s time period.

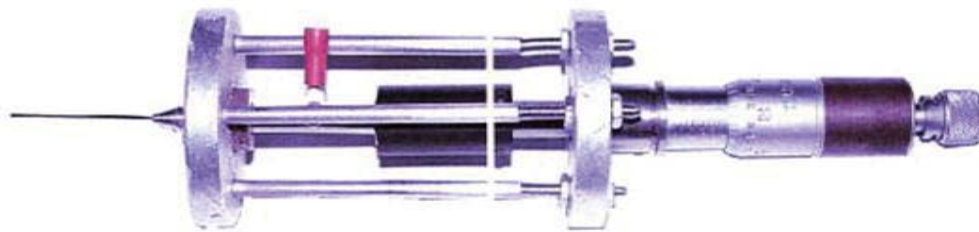


Fig. 5. Film thickness measuring probe.

The thermocouples are connected to a data logger and the temperature data is stored in the personal computer. The surface temperature, inlet feed water temperature, feedwater flow rate, feeder height, falling film thickness distribution around the test tube are measured at different locations. The temperature measurement error is about  $\pm 0.01^\circ\text{C}$ , the flow rate measurement error is about  $\pm 0.001$  kg/s, the pressure measurement error is about  $\pm 0.005$  bar, the measurement error of the length (feeder height, diameter and length of the test tube) is about  $\pm 1.0$   $\mu\text{m}$ , and the film thickness measurement error is about  $\pm 3.0$   $\mu\text{m}$ .

### 3. Results and discussions

Figs. 6–11 show the effect of the treatment of the outside tube surface by plasma irradiation on the thickness

variations of a falling film ( $\delta$ ) with changes of feeder height ( $z$ ), excess temperature ( $\Delta T_e$ ), inlet water subcooling ( $\Delta T_{\text{sub}}$ ), tube diameter ( $d_{\text{ot}}$ ), falling water flow rate, and evaporation pressure ( $p_v$ ) respectively. From these figures, it can be seen that the film thickness of the tube first decreases, and then increases as the peripheral angle increases. The water flows downward along the perimeter of the tube wall associated with the combined forces of gravity, inertia and viscous. The liquid reaches the top of the tube at a certain inertia force. As the peripheral angle increases, the tangential component of gravity increases. The liquid film flow rate increases continuously as does the inertial force of the liquid film increases as the peripheral angle ( $\theta$ ) increases from  $0^\circ$  to  $90^\circ$  and thus the presence of waves on the thin liquid film increases, leading to an increase in the interface region and the convective heat transfer.

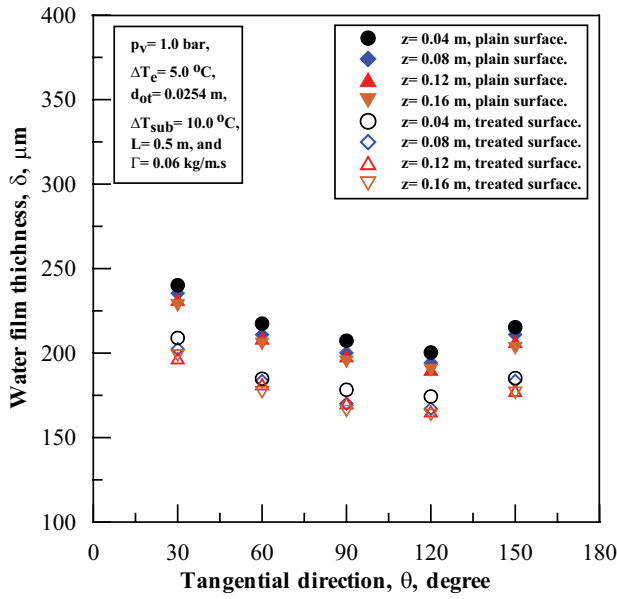


Fig. 6. Effect of the feeder height on the film thickness.

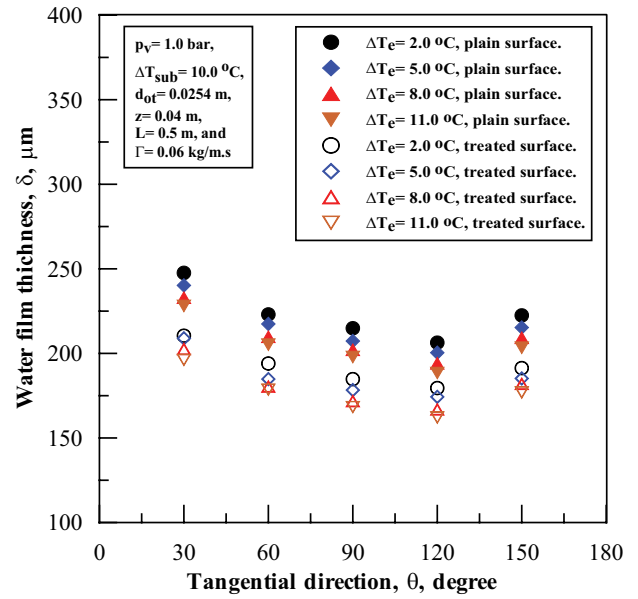


Fig. 7. Effect of the surface temperature on the film thickness.

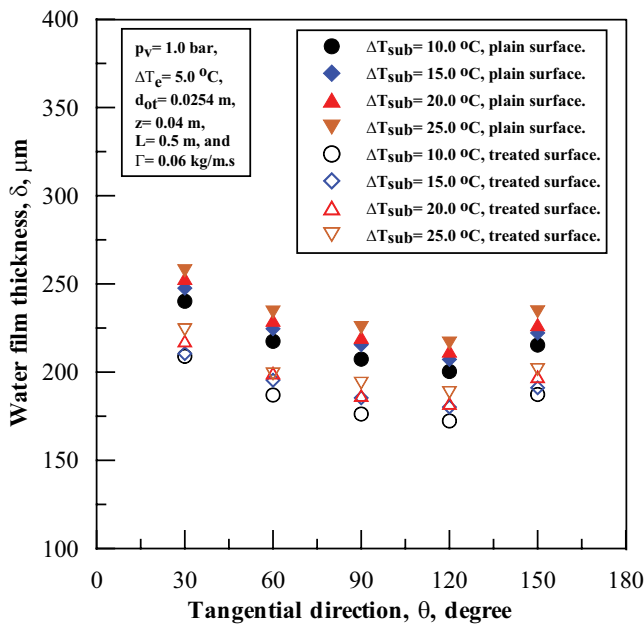


Fig. 8. Effect of the inlet water subcooling on the film thickness.

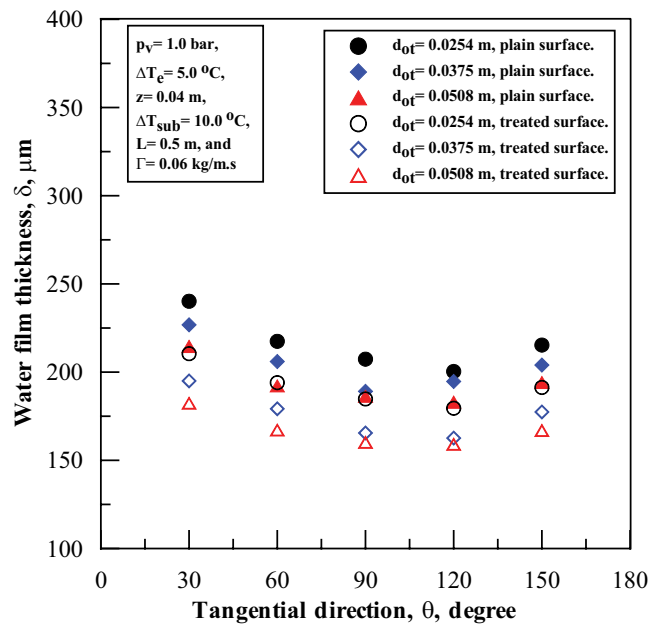


Fig. 9. Effect of the tube diameter on the film thickness.

In addition, the increase in the flow rate of the liquid film contributes to an increase in the viscous force on the tube wall. However, at the peripheral angle ranged from 0° to 90°, the liquid film flow rate increases and the thickness of the liquid film decreases. This is because the summation of gravity's tangential component and inertial forces is always greater than the viscous force. After the liquid film flows to the peripheral angle greater than 90°, the tangential gravity component gradually decreases as the peripheral angle continues to increase. The summation of the tangential component of gravity and inertial force is still greater than the viscous force so that the film thickness

continues to decrease. As the peripheral angle gradually increases, the viscous force continually increases; while the sum of the tangential component of gravity and inertial forces gradually decreases. At a certain peripheral angle between 90° and 120°, the summation of gravity's tangential component and inertial force equals the viscous force, at this angle the peripheral thickness of a liquid film reaches the minimum value. With the further increase of peripheral angle, the summation of gravity's tangential component and inertial forces is always less and therefore than the viscous force, so that the film thickness continues to increase. The film thickness around the hydrophilic tube changes

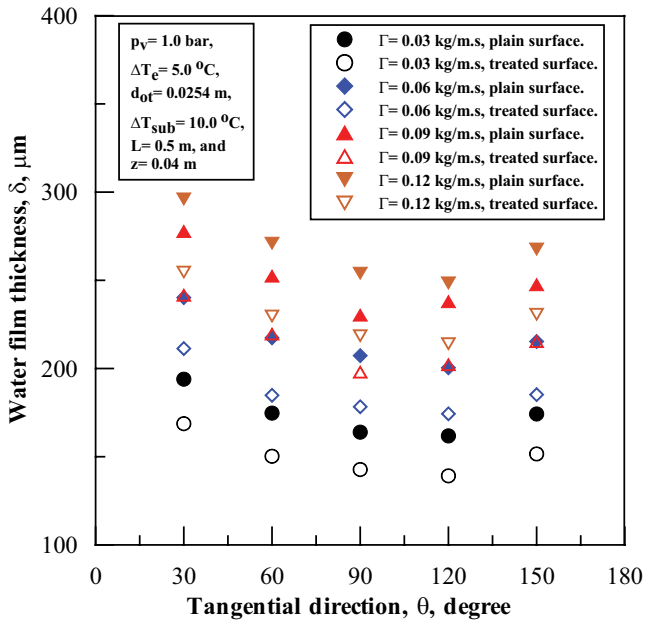


Fig. 10. Effect of the feed flow rate on the water film thickness.

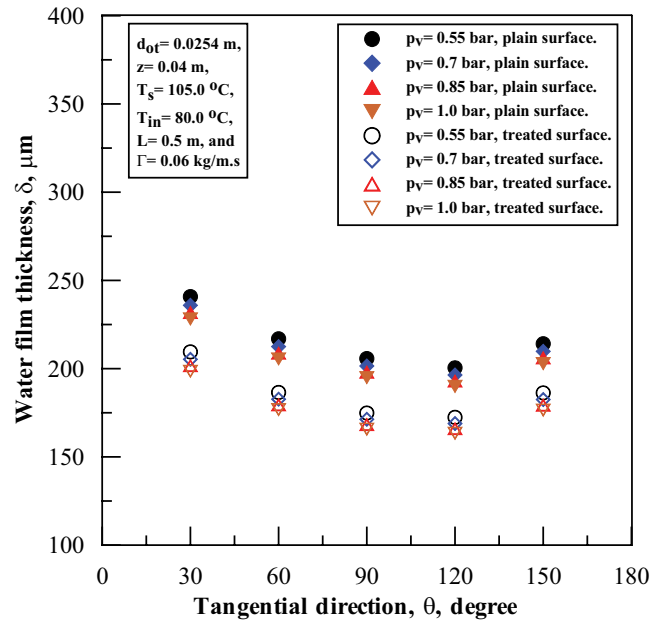


Fig. 11. Effect of the evaporation pressure on the water film thickness.

with the same pattern as around the plain tube. The film is unsymmetrically distributed along the peripheral angle, and the minimum values of the film thickness will in general situate at the angular position of 90°–120°. The falling film thickness decreases from the top angular position to  $\theta$  approximately 90°–120° and subsequently increases again to  $\theta$  approximately 150° where it disconnects. The present results are in line with the results obtained by researchers [15–20], which indicate that film distribution along the peripheral angle is non-symmetrical, and the minimum film thickness values are more likely to appear at different angular. The film thickness is significantly reduced with surface treatment due to the impact of surface cleaning, where the surfaces treated hydrophilically by plasma irradiation are highly ideal and completely safe from any asperities on the surfaces. The falling film-solid contact angle significantly decreases for the surfaces hydrophilically treated by plasma irradiation, Negeed et al. [6]. The falling film tends to spread as the contact angle becomes small (for surfaces treated by plasma irradiation). This is because the contact area between the falling liquid and the heating surface during the first stage of the collision of the falling liquid increases, which is associated with enhanced conduction heat transfer, therefore the film thickness significantly decreases.

Fig. 6 shows the effect of feeder height ( $z$ ) on the thickness variations of a falling film ( $\delta$ ) around the plain and hydrophilic horizontal tube evaporator surfaces. It can be seen that the feeder height has a little impact on the falling film thickness; the water layer thickness slightly decreases as the feeder height increases at the same peripheral angle and the Reynolds number of the liquid film. This is due to the increase in the volatilization of the falling flow rate as the feeder height increases, actually, the thickness of the film decreases with the reduction of the accumulated liquid extending along the tube wall. The present results are in line with the results acquired by Hu

and Jacobi [21], Chyu and Bergles [22], Zhao et al. [15], and Awad and Negeed [9,10], called attention to a powerless impact of the feeder height on the heat transfer coefficient of the falling film in the boiling conditions.

Fig. 7 shows the effect of excess temperature ( $\Delta T_e$ ), the difference between the tube surface and the saturation temperatures, on the falling film thickness ( $\delta$ ) around the plain and hydrophilic horizontal tube evaporator surfaces at various angular positions. It can be seen from this figure that, the water layer thickness slightly decreases as the excess temperature increases. This is because the bubbling nucleate is improved by increasing the  $\Delta T_e$  and the formation of bubbles at the heated tube surfaces will increase. Also, the viscous force is decreased by increasing the excess temperature and the consequent reduction in film thickness. The present results are in line with the results obtained by Parken et al. [23], showing that under boiling-dominated conditions, the heat transfer coefficient increases as the heat flux increases. This behavior is obviously due to increased nucleation site density and increased boiling region.

Fig. 8 shows the impact of the inlet water subcooling ( $\Delta T_{sub}$ ), the difference between the saturation and inlet water temperatures, on the falling film thickness ( $\delta$ ) around the plain and hydrophilic horizontal tube evaporator surfaces at various angular positions. From this figure, it can be seen that the falling film thickness decreases as the  $\Delta T_{sub}$  decreases. This is due to the effect of the decrease in viscous force associated with the rise in bulk temperature and the consequent reduction in film thickness.

Fig. 9 shows the effect of the tube diameter ( $d_{ot}$ ) on the falling film thickness ( $\delta$ ) around the plain and hydrophilic horizontal tube evaporator surfaces at various angular positions. It can be seen from this figure that the water layer thickness decreases as the tube size increases. This is because

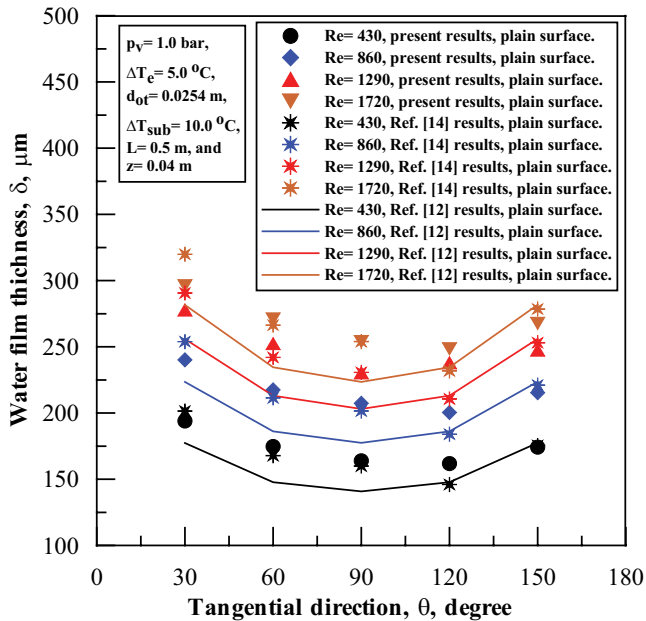


Fig. 12. Comparison between the present results and the results obtained by other researchers for the impact of falling water Reynolds number on the water layer thickness.

the heat transfer enhances as the size of the tube increases in the presence of bubble nucleation, as the thermal profile improvement enables the growth of bubbles. The larger the tube diameter, the greater the number of interface waves presented on the thin liquid film that has a strong effect on the rate of evaporation since the interface region is increased and the convective heat transfer near the interface is thus enhanced. Thus the liquid film's flow rate becomes small, leading to a slight increase in film thickness. The present results agree with the results gained by Abraham and Mani [24] and Zhao et al. [15], where they showed the falling film thickness decreases as extending the tube size. Tube diameter overall influences the falling film thickness because it affects the length of the thermal boundary layer development and the length of the liquid impingement region compared to the overall flow length.

Fig. 10 shows the effect of falling water flow rate per one side of the hot tube surface ( $\Gamma$ ) on the falling film thickness ( $\delta$ ) around the flat and hydrophilic horizontal evaporator tube surfaces at different angular positions. From this figure, it can be seen that the thickness of the water film increases primarily as the  $\Gamma$  increases at the same peripheral angle. This is due to the increase in the accumulated liquid extending along the tube wall as the falling water flow rate increases, and the increase in the viscous force. Generally, the falling water flow rate influences the falling film thickness because it affects the length of the thermal boundary layer development and the length of the liquid impingement region compared to the overall flow length. As the number of Reynolds increases, the inertia force increases and the coefficient of film heat transfer also increases in the presence of bubble nucleation due to the increase of the relative region of active boiling; as the improvement in the thermal profile allows the growth of bubbles. The present results agree with

the results obtained by Abraham and Mani [24], where they observed the increase in the number of film Reynolds leading to an increase in film thickness.

Fig. 11 shows the effect of evaporation pressure ( $p_v$ ) on the falling film thickness ( $\delta$ ) around the plain and hydrophilic horizontal tube evaporator surfaces at various angular positions. From this figure, it can be seen that the falling film thickness slightly increases as the  $p_v$  decreases. This is due to the effect of increasing the viscous force associated with decreasing the evaporation pressure and the consequent rise in the thickness of the film.

Fig. 12 shows the comparison of the current results with the results obtained by Nusselt [12] and Hou et al. [14] for the impact of the water falling Reynolds number ( $Re$ ) on the thickness of the liquid surface ( $\delta$ ) around the plain horizontal tube evaporator surfaces. It can be seen from this figure that the thickness of the water film increases primarily as the number of Reynolds increases. This is due to the increase in the accumulated liquid extending along the tube wall as the falling water flow rate increases, and the increase in the viscous force. It is the current results the minimum values of film thickness are more likely to be found at the angular location of  $120^\circ$  under various conditions. The falling film thickness decreases from the top angular position to approximately  $120^\circ$  and subsequently increases again to about  $150^\circ$  where it is detached. The present results are in line with the results obtained by Hou et al. [14], the film was unsymmetrically distributed along the peripheral angle as shown in the figure. In the results obtained by Nusselt [12], the falling film thickness decreases from the top angular position to equals  $90^\circ$  and then increases again up to  $\theta$  approximately equals  $160^\circ$  where it detaches. The comparison between the current results and results acquired by Nusselt [12] and Hou et al. [14] is in good agreement between 2.0 and 18%.

#### 4. Conclusions

Water falling film around plain and hydrophilic horizontal tube evaporator surfaces was experimentally conducted to investigate the effect of operating conditions and evaporator design on the formed film thickness around the evaporator tube surfaces. From this study, the following conclusions can be drawn: the film thickness significantly decreases for hydrophilic surfaces. Around the hydrophilic tube, the film thickness varies with a pattern similar to that around the plain tube. The film is unsymmetrically distributed along the peripheral angle. The falling film thickness decreases from the top angular position to  $\theta$  approaches  $90^\circ$ – $120^\circ$ , and afterward increases again up to  $\theta$  roughly rises to  $150^\circ$  where it disconnects. For the plain and hydrophilic surfaces, the film thickness mainly increases as the flow rate increases, while it decreases as the tube size increases, the evaporation pressure increases, the inlet water subcooling increases, and tube surface temperature increases. The feeder height has little effect on the film thickness. The comparison between the current results and results acquired by another researcher is in good agreement between 2.0 and 18 percent. The present work provides experimental valuable data that can be used for the validation of computational fluid dynamics studies of the thickness variations of a falling film on plain and hydrophilic

horizontal tube evaporator surfaces in order to enhance the performance of the horizontal tube evaporators.

## Symbols

|                    |  |
|--------------------|--|
| $d_{ot}$           | — Outer diameter of the test tube, m   |
| $g$                | — Gravitational acceleration, m <sup>2</sup> /s  |
| $L$                | — Tube length, m   |
| $p$                | — Pressure, N/m <sup>2</sup>   |
| $p_v$              | — Evaporator pressure, N/m <sup>2</sup>  |
| Re                 | — Reynolds number, –   |
| $s$                | — Tube spacing, m  |
| $T$                | — Temperature, K   |
| $T_{in}$           | — Inlet water temperature, K   |
| $T_s$              | — Tube surface temperature, K  |
| $T_s^{sat}$        | — Saturation temperature, K  |
| $\Delta T_e^{sat}$ | — Excess temperature (the difference between the tube surface and the saturation temperatures), K                  |
| $\Delta T_{sub}$   | — Inlet water subcooling (the difference between the saturation and inlet water temperatures), Kz feeder height, m |

## Greek

|          |   |
|----------|---|
| $\Gamma$ | — Liquid film flow rate on one side of the tube per unit length sprayed, kg/s m |
| $\delta$ | — Film thickness, m   |
| $\theta$ | — Peripheral angle from the upper stagnation point, degree                      |
| $\mu$    | — Dynamic viscosity kg/s m  |
| $\rho$   | — Density, kg/m <sup>3</sup>  |

## Subscripts

|     |                               |
|-----|-------------------------------|
| $e$ | — Excess                      |
| in  | — Inlet falling water         |
| $l$ | — Saturated liquid conditions |
| ot  | — Outer tube surface          |
| $s$ | — Surface conditions          |
| sat | — Saturation conditions       |
| $v$ | — Saturated vapor conditions  |

## References

- [1] C.-Y. Zhao, W.-T. Ji, P.-H. Jin, W.-Q. Tao, Heat transfer correlation of the falling film evaporation on a single horizontal smooth tube, *Appl. Therm. Eng.*, 103 (2016) 177–186.
- [2] B. Narváez-Romo, J.R. Simões-Moreira, Falling liquid film evaporation in subcooled and saturated water over horizontal heated tubes, *Heat Transfer Eng.*, 38 (2017) 361–376.
- [3] H. Hou, Q.C. Bi, X.L. Zhang, Numerical simulation and performance analysis of horizontal-tube falling-film evaporators in seawater desalination, *Int. Commun. Heat Mass Transfer*, 39 (2012) 46–51.
- [4] G. Ribatski, A.M. Jacobi, Falling-film evaporation on horizontal tubes—a critical review, *Int. J. Refrig.*, 28 (2005) 635–653.
- [5] W.-M. Yan, C.-W. Pan, T.-F. Yang, M. Ghalambaz, Experimental study on fluid flow and heat transfer characteristics of falling film over tube bundle, *Int. J. Heat Mass Transfer*, 130 (2019) 9–24.
- [6] E.-S.R. Negeed, M. Albeirutty, S.F. AL-Sharif, S. Hidaka, Y. Takata, Dynamic behavior of a small water droplet impact onto a heated hydrophilic surface, *J. Heat Transfer*, 138 (2016) 1–11, <https://doi.org/10.1115/1.4032147>.
- [7] E.-S.R. Negeed, M. Albeirutty, Y. Takata, Dynamic behavior of micrometric single water droplets impacting onto heated surfaces with TiO<sub>2</sub> hydrophilic coating, *Int. J. Therm. Sci.*, 79 (2014) 1–17.
- [8] M.W. Shahzad, A. Myat, W.G. Chun, K.C. Ng, Bubble-assisted film evaporation correlation for saline water at sub-atmospheric pressures in horizontal-tube evaporator, *Appl. Therm. Eng.*, 50 (2013) 670–676.
- [9] M.M. Awad, E.-S.R. Negeed, Heat transfer enhancement of falling film evaporation on a horizontal tube bundle, *Int. J. Nucl. Desal.*, 3 (2009) 283–300.
- [10] E.-S.R. Negeed, M.M. Awad, Experimental study of falling film evaporation on horizontal tube bundle for a desalination unit, *Int. J. Nucl. Desal.*, 4 (2010) 1–17.
- [11] E.-S.R. Negeed, Enhancement of the performance of the vapour compression plant, *Int. J. Nucl. Desal.*, 4 (2010) 88–108.
- [12] W. Nusselt, Die oberflächenkondensation des wasserdampfes, *Zeitschrift des Vereines Deutscher Ingenieure*, 60 (2016) 541–575.
- [13] M.-C. Chyu, A.E. Bergles, An analytical and experimental study of falling-film evaporation on a horizontal tube, *ASME J. Heat Transfer*, 109 (1987) 983–990.
- [14] H. Hou, Q.C. Bi, H. Ma, G. Wu, Distribution characteristics of falling film thickness around a horizontal tube, *Desalination*, 285 (2012) 393–398.
- [15] Y. Zhao, D. Wang, Y. Liu, M. Tang, S.F. Zhang, Distribution characteristics of falling film thickness around a horizontal corrugated tube, *Int. J. Heat Mass Transfer*, 154 (2020) 119773, <https://doi.org/10.1016/j.ijheatmasstransfer.2020.119773>.
- [16] Y.H. Zhou, Z. Cai, Z. Ning, M.S. Bi, Numerical simulation of double-phase coupled heat transfer process of horizontal-tube falling film evaporation, *Appl. Therm. Eng.*, 118 (2017) 33–40.
- [17] C.-Y. Zhao, W.-T. Ji, P.-H. Jin, P.-H. Zhong, W.-Q. Tao, Hydrodynamic behaviors of the falling film flow on a horizontal tube and construction of new film thickness correlation, *Int. J. Heat Mass Transfer*, 119 (2018) 564–576.
- [18] X. Chen, S.Q. Shen, Y.X. Wang, J.X. Chen, J.S. Zhang, Measurement on falling film thickness distribution around horizontal tube with laser-induced fluorescence technology, *Int. J. Heat Mass Transfer*, 89 (2015) 707–713.
- [19] A. Jayakumar, A. Balachandran, A. Mani, K. Balasubramaniam, Falling film thickness measurement using air-coupled ultrasonic transducer, *Exp. Therm. Fluid Sci.*, 109 (2019) 109906, <https://doi.org/10.1016/j.expthermflusci.2019.109906>.
- [20] L.-C. Luo, G.-M. Zhang, J.-H. Pan, M.-C. Tian, Flow and heat transfer characteristics of falling water film on horizontal circular and non-circular cylinders, *J. Hydrodyn. Ser. B*, 25 (2013) 259–270.
- [21] X. Hu, A.M. Jacobi, The intertube falling film: Part 2—mode effects on sensible heat transfer to a falling liquid film, *J. Heat Transfer*, 118 (1996) 626–633.
- [22] M.-C. Chyu, A.E. Bergles, An analytical and experimental study of falling-film evaporation on a horizontal tube, *J. Heat Transfer*, 109 (1987) 983–990.
- [23] W.H. Parken, L.S. Fletcher, V. Sernas, J.C. Han, Heat transfer through falling film evaporation and boiling on horizontal tubes, *J. Heat Transfer*, 112 (1990) 744–750.
- [24] R. Abraham, A. Mani, Heat transfer characteristics in horizontal tube bundles for falling film evaporation in multi-effect desalination system, *Desalination*, 375 (2015) 129–137.